Published in AJSE, Vol: 24, Issue:2
Received on 27th December 2024
Revised on 4th May 2026
Published on 31th May 2026

AIUB JOURNAL OF SCIENCE AND ENGINEERING
ISSN: 1608 - 3679 (print) 2520 - 4890 (Online)
https://doi.org/10.53799/0wst4325

A Compact Meandered Monopole Antenna with Controlled Frequency Reconfiguration for LoRa IN865 and AS923-3 Bands

Chaya Devi Pothala and Ramarakula Madhu

***Abstract*— The global demand for compact and low power IoT devices is rapidly increasing, particularly in countries like India and those in South Asia. Low Power Wide Area Networks (LPWANs) equipped with LoRa antennas are well-suited to address this need. Most existing LoRa antennas are multiband microstrip designs with the operating bands usually limited to one of the LoRa bands AS923-1, EU868, IN865, and RU864, along with other sub-GHz ranges. In this paper, we present a compact, low-cost, reconfigurable Meandered Monopole antenna (MMA) designed to operate only in the LoRa IN865 and AS923-3 bands. To keep the antenna compact and economical, a meandered monopole structure has been employed with an RF PIN diode on an FR-4 substrate. Unlike existing designs, the proposed antenna is accurately tuned and is dedicated solely to the LoRa frequency band. The design was simulated using CST Microwave Studio (CST-MWS) and validated through prototype measurements. Furthermore, a unique lumped equivalent circuit model was developed using Keysight ADS. The proposed antenna has shown good pattern stability and achieves a gain of 2.07 dBi. With the diode in the active (ON) state, the antenna resonates at 866.2 MHz (IN865 LoRa Band) with an S11 of -17.22 dB and Bandwidth of 19 MHz. In the inactive (OFF) state of the diode, the antenna resonates at 916.5 MHz (AS923-3 LoRa Band) with an S11 of -15.24 dB and Bandwidth of 22 MHz. The results confirm that the proposed antenna provides reliable reconfigurability for LoRa applications in the specified bands.**

***Index Terms*—LoRa-IoT, IN865, AS923-3, Reconfigurable Antenna, Meandered Monopole, ADS Keysight, CST Microwave studio**

I. Introduction

In the age of intelligent gadgets, there is an increasing need for communication technologies that provide long distance communication with affordable pricing and employs energy-efficient techniques. LPWANs because of versatile, energy-efficient, and long-distance communication infrastructure have emerged as a vital option to address this requirement in the applications of Internet of Things (IoT) [1]. According to [2] there will be an 267.8% growth in usage of IoT devices in India and South Asia followed by 197.14% growth in East Asia with 640% raise in devices enabled with non-mMTC (massive Machine Type Connectivity) LPWA private networks [3]. Hence, LPWANs that rely on LoRa radio as its physical medium protocol proved to be one finest technology in demand addresses the above requirements.

LoRa stands for Long Range and is a sub-GHz wireless technology used to establish communication among LoRa devices with in the unlicensed spectrum [4]. Due to the robustness in communication over long distance with minimal power consumption, it has wide spread applications in the fields of automation, environmental monitoring, smart environment, health care, tracking etc. [3]. The frequency gaps in the Industrial, Scientific, and Medical (ISM) band which do not need regulatory licensing for their usage can be the LoRa band of operation [5]. Unlike, standard technologies such as Bluetooth that works on the globally available unlicensed 2.4 GHz band, LoRa do not have a fixed operating frequency band [6]. It is being operated globally at various frequency bands allowing flexible deployment as per the regional regulations and environmental conditions. The various regional specific dynamic channel plan operating bands of LoRa is shown in table 1 [7].

TABLE I
REGIONAL OPERATING FREQUENCY BANDS FOR LORA

Plan	Region	Default Frequency Band (MHz)	Default Rx_2 receiver Frequency (MHz)
EU868	European Union	863 – 870	869.525
CN779	China	779 – 787	786.0
EU433	European Union	433 – 434	434.665
IN865	India	865 – 867	866.550
KR920	South Korea	920.9 – 923.3	921.90
AS923-1/2/3	Asia	915 – 928	923.2/921.4/916.6
RU864	Russia	864 – 870	869.1

The modulation utilised for effectively managing interference in Lora signals is Chirp Spread Spectrum (CSS) and it guarantees long-distance connection. Furthermore, essential LoRa features such as frequency of carrier (CF), Spreading Factor (SF) and Data rate of code (CR) may be dynamically modified using the Adaptive Data Rate (ADR)

Chaya Devi Pothala
Department of ECE, Anil Neerukonda Institute of Technology and Sciences
Visakhapatnam, Andhra Pradesh, India
pchayadevi@gmail.com

Ramarakula Madhu
Department of ECE, Jawaharlal Nehru Technological University Kakinada
Kakinada, Andhra Pradesh, India
madhu_ramarkula@jntucek.ac.in

method [8]. Apart from its technical aspects, the efficacy of LoRa is closely tied to the functioning of antennas. Optimal LoRa antenna selection provides the most effective transmission, allowing greater connectivity and extended communication capabilities in a variety of situations [9]. This indicates the requirement for power effective, multitasking, and portable IoT devices with antennas of reduced footprint and reconfigurable flexibility.

The existing works relative to LoRa MPAs shows that most of the designs are multiband reconfigurable antennas, out of which only one band operates in LoRa and the other bands have different applications [10], [11], [12], [13], [14], [15], [16], [17], [18], and [19]. The antenna designs are fabricated on an FR-4 substrate have multiple shapes and are operated at LoRa frequency bands (915 MHz, 433 MHz, and, 868 MHz), covering the bands in Asia, Europe, and Russia. These antennas have the footprint around 70 mm by 50 mm and are reconfigurable but designed to support other wireless applications alongside LoRa. However, these designs tend to focus on LoRa bands in the regions outside India, such as Europe and Russia, and the antennas are relatively large.

Considering the substantial rise in demand for internet enabled devices in the regions of India and Asia, this work focuses in design and development of a cost-effective and compact frequency reconfigurable LoRa antenna within the LoRa bands of IN865 (866.5MHz) and AS923-3 (916.6MHz) addressing the current needs of IoT devices in these regions. While the underlying techniques such as meandered monopoles and PIN-diode-based reconfiguration are well established, the contribution of this work lies in their integration to realize a compact, single-diode reconfigurable antenna specifically optimized for LoRa IN865 and AS923-3 bands with reduced design complexity.

The next section presents the design and performance of two base antennas for individual operation in the IN865 and AS923-3 bands. This is followed by the development of a frequency-reconfigurable antenna using a PIN diode, along with parametric tuning of the meandered dipole and stub geometries. The equivalent lumped-element model and a comparison of the simulated and measured performances are then discussed.

II. Design and Development of Base Antenna

The intricate antenna design involves strategically folding the meandered monopoles, a process guided by equations given below and corresponding to the design of meandered patch [21],[22].

$$d_{ml} = 0.16\lambda_g + \partial c \quad (1)$$

$$w_{ml} = 0.05\lambda_g + \partial c \quad (2)$$

$$L_p = 0.70\lambda_g + \partial c \quad (3)$$

$$w_p = 0.42\lambda_g + 2w_{ml} + \partial c \quad (4)$$

Where λ_g is the guided wavelength and is given as

$$\lambda_g = \frac{\lambda}{\sqrt{\epsilon_r^{ef}}}$$

Here λ and ϵ_r^{ef} are the free space wavelength and effective dielectric constant respectively, given as

$$\epsilon_r^{ef} = 0.5\ (\epsilon_r + 1) + \ 0.5\ (\epsilon_r - 1)[1 + 10\frac{S_h}{w_{ml}}] \quad (5)$$

$$\partial c = \frac{0.25C}{f_{res}}\sqrt{\frac{2}{\epsilon_r+1}} \quad (6)$$

Where

d_{ml} the distance between successive meandered segments
w_{ml} the width of meandered segment
L_p the meandered patch length
w_p the meandered patch width
S_h the substrate height
S_l the substrate length
S_w the substrate width
C the velocity of light
ϵ_r the dielectric constant

The equations from 7-8 aid in design of substrate [23]

$$S_w = 6S_h + w_p \quad (7)$$

$$S_l = 6S_h + L_p \quad (8)$$

LoRa frequencies have global classifications, with 866.5 MHz predominantly utilized in India and 916.6MHz favored in the Asian regions. In line to the frequency bands, figure 1.a illustrates the geometry of a basic LoRa meandered monopole antenna simulated in CST-MWS, resonating at a center frequency of 916.5MHz (AS923-3) with an S11 of -15.21dB. Figure 1.b presents a modified antenna geometry, featuring an increased physical length of the meandered monopole patch that is shown in figure 1.a. An additional meandered monopole element, measuring 32mm in width and 1mm in length, is attached to the design given in figure 1.a via a patch measuring 3mm in width and 3mm in length. This modified antenna resonates at a center frequency of 866.1MHz (IN865) with S11 of -13.30dB. The ground plane in both the designs incorporates a defected ground structure, depicted in figure 1.c.

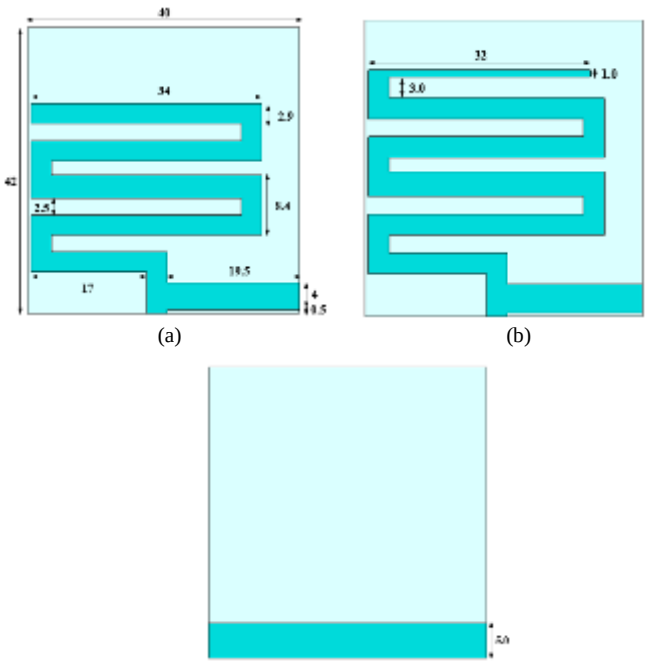

(a) (b)

(c)

Fig. 1. Base antenna design a) Patch geometry for AS923-3 band b) Patch geometry for IN865 band c) Ground plane for AS923-3 & IN865

Parameters such as stub length (SL), stub width (SW), and stub start (SS) have been carefully chosen as 4mm, 19.5mm, and 0.5mm, respectively, to achieve maximum impedance matching at both resonant frequencies. This stub helps in reducing power loss between the antenna and the feed line, thereby ensuring efficient signal transmission and reception. Its incorporation enhances the antenna's overall efficacy, making it well-suited for diverse applications within the specified frequency bands.

The patch is designed on the upper surface of an FR4 substrate, 1.6mm thick, with tanδ = 0.02 and dielectric constant of 4.4. The antenna's performance in terms of gain, VSWR, and S11 at the respective center frequencies has been tabulated in table 2. The return loss observed from simulating the antenna geometries is shown in figure 2. Consequently, the antenna geometry is considered as the basis for designing the proposed frequency reconfigurable antenna for LoRa.

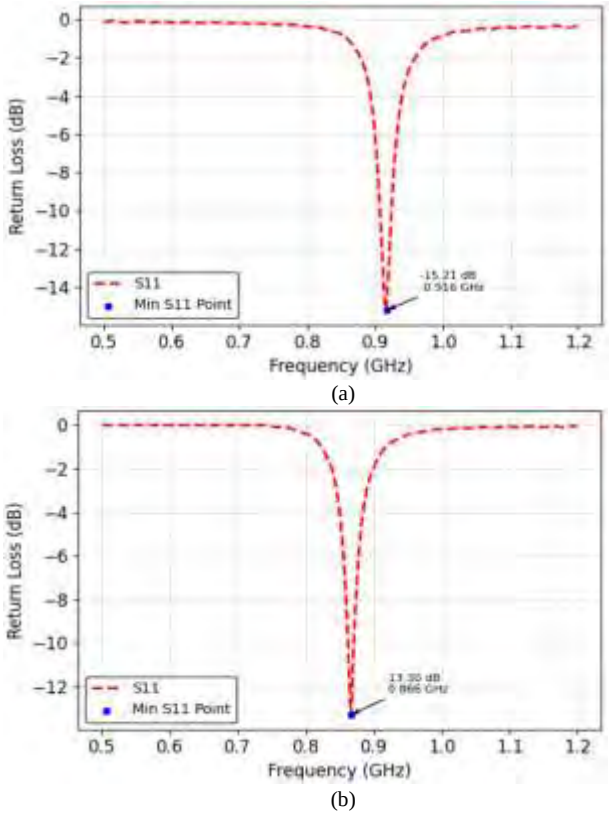

Fig. 2. Simulated return loss of the base antenna design a) AS923-3 band (916.5 MHz) and IN865 Band (866.1 MHz)

TABLE II
PERFORMANCE METRICS OF THE BASE ANTENNA DESIGNS

Resonant frequency	916.5 MHz	866.1 MHz
S11	-15.21 dB	-13.30 dB
Gain	2.07 dB	2.05 dB
VSWR	1.42	1.38

III. DESIGN AND DEVELOPMENT OF PROPOSED ANTENNA

This section presents the design of the proposed reconfigurable antenna, which is specifically engineered to operate within the IN865 and AS923-3 LoRa frequency bands. To achieve compact dual-band performance in the UHF range, meandered radiating structures and folded inverted-F antennas are commonly employed due to their space-efficient characteristics. Leveraging these principles, the antenna designs discussed in the previous section form the basis for the development of the proposed antenna.

The primary aim is to combine the two designs and seamlessly switch between the designs, a task made possible by the integration of a single RF PIN Diode (BAR50-02V) manufactured by Infineon. The antenna design shown in figure 3 has been reciprocated from the base antenna designs and the parameters W6 and L6 are meticulously determined to ensure resonance in both IN865 and AS923-3 LoRa bands, depending on the mode of the diode. The detailed design, tuning, and analysis are conducted using CST-MWS software, with excitation accomplished through a microstrip feed line measuring 3 mm in width.

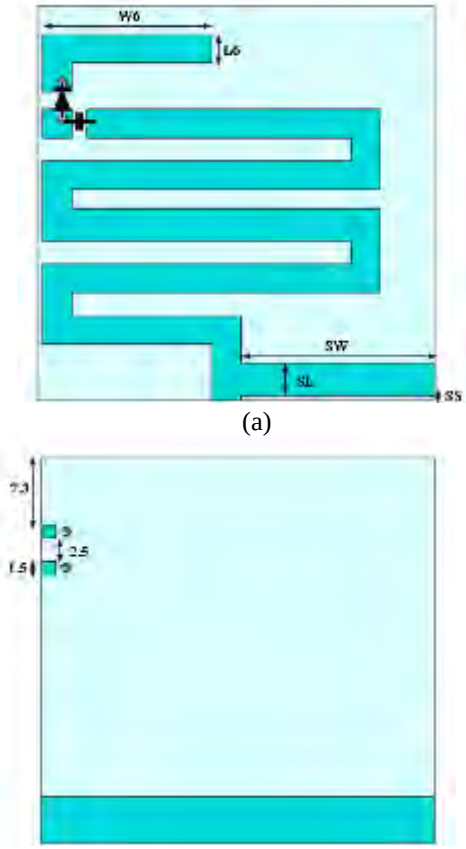

Fig. 3. Proposed antenna design a) Patch b) Ground plane

The lumped equivalent model of the PIN Diode during its active and inactive states and its biasing circuit is given in figure 4. During forward biasing, the opposition offered to the change in current by the diode at high frequencies, is represented with series combination of an inductor and a resistor. In reverse bias, PIN Diode acts as a capacitor controlled variable resistor and its behaviour at high frequency operation can be approximated with the model shown in figure 4b and the biasing of PIN Diode is shown in figure 4c.

The biasing network, comprising bias lines, RF chokes, and DC blocking capacitors, is represented using lumped element models rather than explicit electromagnetic structures

in CST-MWS simulations. At sub-GHz frequencies (866-916 MHz), these components are electrically small relative to the operating wavelength and therefore have a negligible influence on the antenna radiation characteristics. Hence, their effects are incorporated through equivalent lumped elements that capture the relevant parasitic RLC behavior, as presented in Section IV, without introducing additional computational complexity.

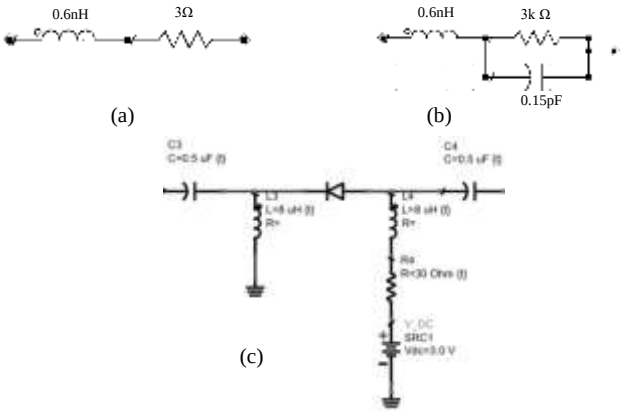

Fig. 4. Lumped equivalent model of the PIN diode (BAR50-02V)
a) Active state b) Inactive state c) Biasing circuit of the PIN diode

IV. Parametric Optimization of Proposed Antenna

The design was optimised in two stages. Initially, the parametric sweep of L6 and W6 was performed to set the fundamental resonant frequencies (866 and 916 MHz). After optimising these parameters, the stub parameters (SS, SL, SW) were tuned to refine impedance matching and mitigate the reactive effects of the PIN diode. This approach is standard in antenna design that separates resonance control from matching optimization [24].

A. Parametric optimisation of Dipole element (L6, W6)

The parameters L6 and W6 were opted as they directly govern the fundamental resonance and impedance behavior of the antenna. From Eq.3, it is evident that L_p is proportional to λg, which depends on the effective dielectric constant ϵ_r^{ef}. Increasing L6 extends the current path (L_p), and results in increasing λg and lowering in the resonant frequency (fres). Similarly, W6 influences both the total patch width W_p and ϵ_r^{ef}. According to Eq.5, a wider dipole slightly reduces ϵ_r^{ef}, increasing λg, and produces minor downward shifts in fres while primarily improving impedance matching.

The parametric optimization of the dipole element dimensions (L6, W6) is carried out while keeping the geometry of the stub and meandered monopoles identical to that of the base antenna. During this process, the parameter W6 is varied from 16 mm to 18 mm, and L6 is varied from 1 mm to 3 mm. The effect of these variations on the return loss under the Diode ON and OFF states is illustrated in figure 5, while the corresponding resonant frequency and return loss values are summarized in table 3.

From the table it is observed that varying L6 and W6 results in minor changes in S11, with values remaining between -17 and -18 dB in the diode ON state and around -22 to -24 dB in the OFF state. However, the diode's presence consistently degrades impedance matching, as seen by the higher S11 values when the diode is active. Therefore, the stub parameters (SS, SL, SW) are tuned next to compensate for the diode's effects and achieve optimal matching.

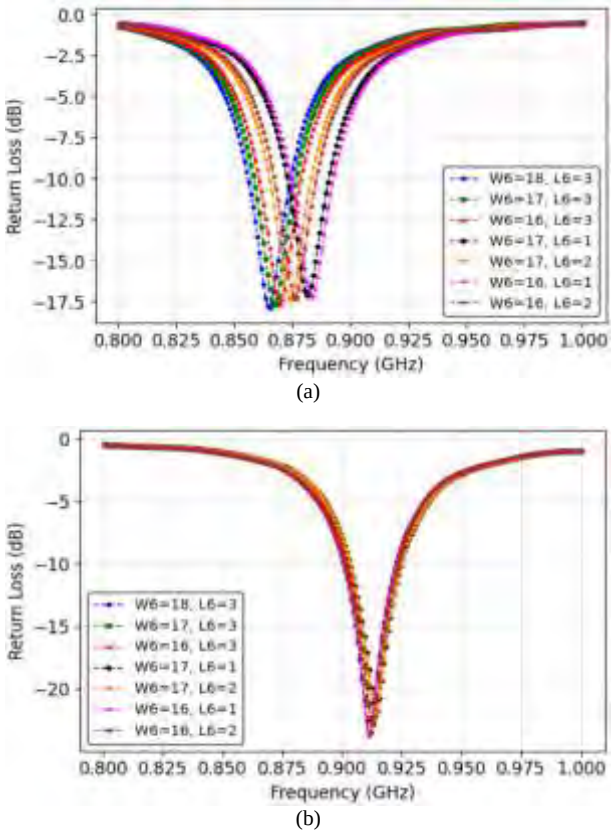

Fig. 5. Effect of L6 and W6 variations on S11 a) diode ON b) diode OFF

TABLE III
Effect of L6 and W6 on Antenna Resonant Frequency and Return Loss

L6 (mm)	W6 (mm)	Diode ON		Diode OFF	
		f_{res} (MHz)	S11 (dB)	f_{res} (MHz)	S11 (dB)
1	16	883.2	-17.2	916.8	-21.8
1	17	881.4	-17.1	916.8	-21.9
2	16	876.0	-17.3	915.9	-22.7
2	17	874.2	-17.4	915.9	-22.8
3	16	869.7	-17.6	915.0	-23.5
3	17	867.0	-17.7	914.2	-23.6
3	18	866.1	-17.9	914.1	-23.7

B. Parametric optimisation of Stub (SS, SL, SW)

Considering the optimal values of L6 and W6 to be 3 mm and 18 mm, respectively, the variation of the stub geometry and its effect on the S11 parameter and resonant frequency are illustrated in figure 6, while the corresponding numerical values are provided in table 4.

It is observed that when the stub parameters SS, SL, and SW are set to 0.5 mm, 4 mm, and 19 mm, respectively, the antenna resonates at 866.2 MHz with an S11 of -17.22 dB in the diode ON state. In the diode OFF state, the antenna resonates at 916.5 MHz with an S11 of -15.24 dB.

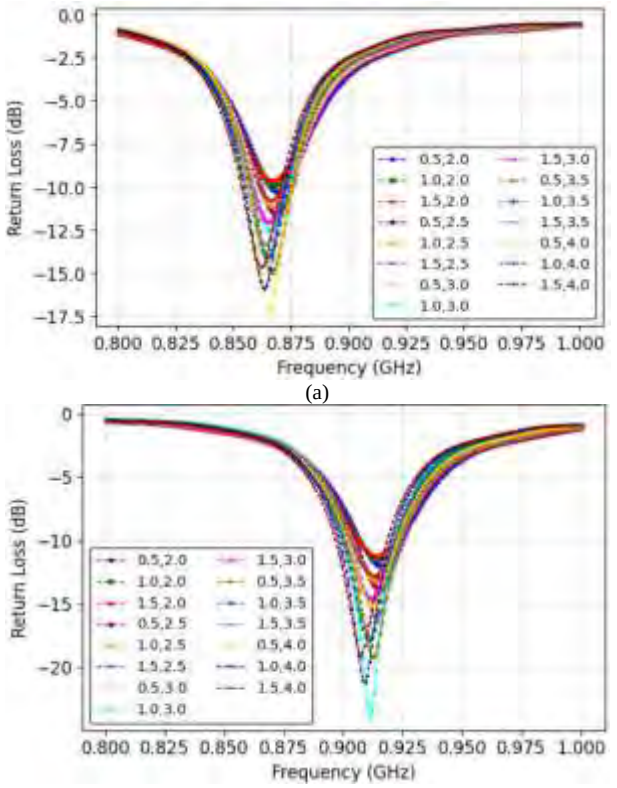

(a)

(b)

Fig. 6. Effect of stub geometry on return loss a) diode ON b) diode OFF

TABLE IV
EFFECT OF STUB GEOMETRY ON ANTENNA RESONANT FREQUENCY AND RETURN LOSS

SS (mm)	SL (mm)	SW (mm)	Diode ON		Diode OFF	
			f_{res} (MHz)	S11 (dB)	f_{res} (MHz)	S11 (dB)
0.5	2.0	19.0	868.8	-10.3	916.5	-11.7
1.0	2.0	19.0	867.9	-9.9	914.7	-10.9
1.5	2.0	19.0	867.0	-9.6	915.6	-13.4
0.5	2.5	19.0	868.8	-11.6	914.7	-15.6
1.0	2.5	19.0	867.0	-11.1	912.0	-14.2
1.5	2.5	19.0	866.1	-10.8	912.9	-18.4
0.5	3.0	19.0	867.9	-13.1	912.0	-22.5
1.0	3.0	19.0	866.1	-12.5	908.4	-18.2
1.5	3.0	19.0	865.2	-12.0	915.6	-12.0
0.5	3.5	19.0	867.0	-15.0	914.7	-13.8
1.0	3.5	19.0	864.3	-14.1	912.9	-12.8
1.5	3.5	19.0	863.4	-13.4	913.8	-16.1
0.5	**4.0**	**19.0**	**866.2**	**-17.2**	**916.5**	**-15.2**
1.0	4.0	19.0	863.4	-15.9	909.3	-16.8
1.5	4.0	19.0	861.6	-14.7	911.1	-23.8

C. Lumped Equivalent Model

Representing the antenna with its RLC lumped equivalent model aids in easier analysis of antenna behavior, reduced simulation times, and seamless integration with other circuit components in design processes. The lumped equivalent model of the proposed antenna is given in figure 7. The model was simulated in Keysight ADS and the simulated S parameter behavior of the model over the frequency range 100MHz to 10GHz is shown in figure 8. The model has been terminated with a 50Ω input impedance network to match to the impedance of a microstrip feed line. This enables maximum power transfer from the input port to the radiating patch. The values $R_0L_0C_0$, L_1 and C_1 are carefully identified to resonate within AS923-3 band, while the $R_2L_2C_2$, L_5 and C_4 resonate the antenna in IN865 band. The inductor L_6 compensates impedance mismatching if any introduced by the biasing components of the diode. In the circuit, the resistor R_4 is used to provide the bias current. The input matching and output matching is provided with L_4, C_4 and L_3, C_3 respectively. Also, the return path to the dc bias current is provided through L_6. The Lumped model simulated results show that the antenna resonates with in the desired LoRa operating Bands and aligns with the CST-MWS simulated model behavior.

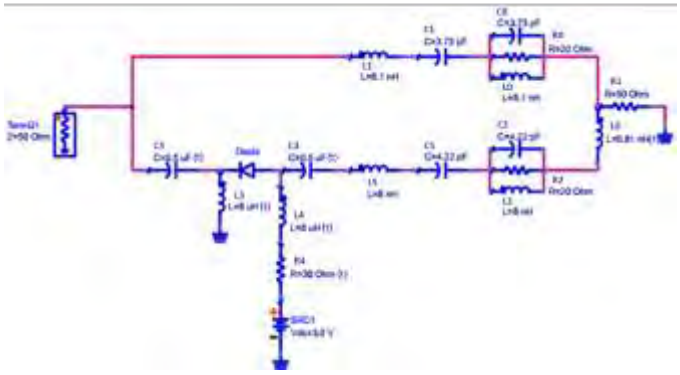

Fig. 7. RLC lumped equivalent model of the proposed antenna

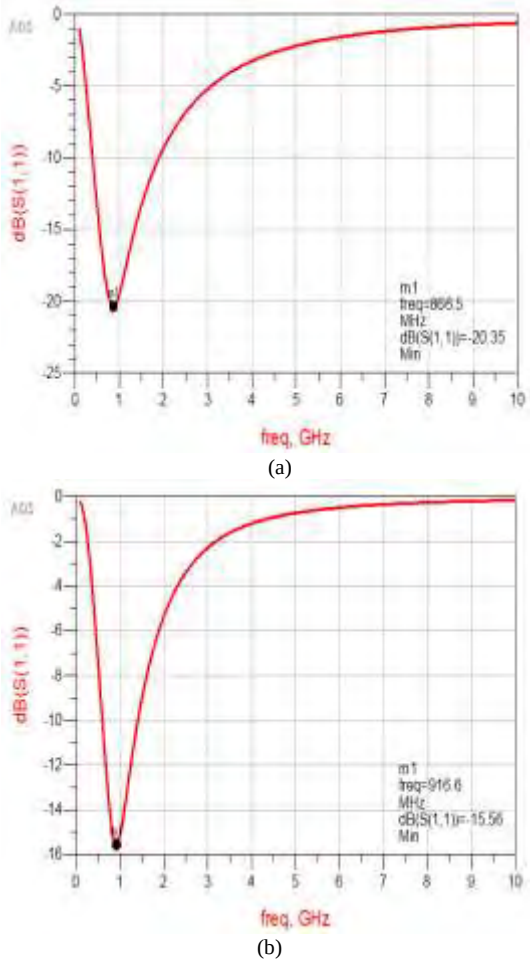

(a)

(b)

Fig. 8. Return loss of lumped equivalent model a) diode ON b) diode OFF

The values of the lumped elements in the equivalent circuit model were determined through a systematic extraction and optimization process. Initially, the resonant frequencies obtained from CST simulations were used to estimate the inductance and capacitance values based on standard LC resonance relations. The resistance components were approximated from the impedance matching characteristics in the simulated S11 response. Following this initial estimation, the circuit parameters were refined using optimization in Keysight ADS to closely match the S11 characteristics of the CST model.

D. Performance Measure of Prototype Antenna

The proposed antenna with its optimized geometry is fabricated, and the prototype is shown in figure 9. A Keysight Vector Network Analyzer (VNA, P5003A) is used to measure the antenna characteristics. A comparison between the measured and simulated S11 parameters is presented in figure 10, showing that both results exhibit closely matching performance. It is observed that when the diode is in the active state, the prototype antenna resonates at 866.8 MHz within the IN865 LoRa band, with an S11 -15.32 dB. Conversely, when the diode is in the inactive state, the antenna resonates at 916.9 MHz within the AS923-3 band, with an S11 of -14.38 dB. Furthermore, the antenna performance at various stages of the design process is summarized in table 5, indicating that the resonant frequency remains stable throughout the different design stages, with only minimal variations observed in the return loss.

Fig. 9. Fabricated prototype of the proposed antenna a) Front plane b) Ground plane

TABLE V
RESONANT FREQUENCY AND S11 AT DIFFERENT STAGES OF THE DESIGN PROCESS

Design Process	**Measurement Technique**	**Diode ON**		**Diode OFF**	
		f_{res} (MHz)	**S11 (dB)**	**f_{res} (MHz)**	**S11 (dB)**
Base design	CST-MWS	866.1	-13.30	916.5	-15.21
Proposed reconfigurable design	CST-MWS	866.2	-17.22	916.5	-15.24
Proposed design – Lumped model	ADS	866.5	-20.35	916.6	-15.56
Prototype of the design	VNA	866.8	-15.32	916.9	-14.38

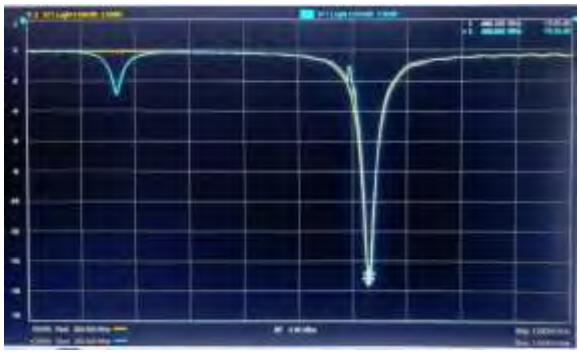

(a)

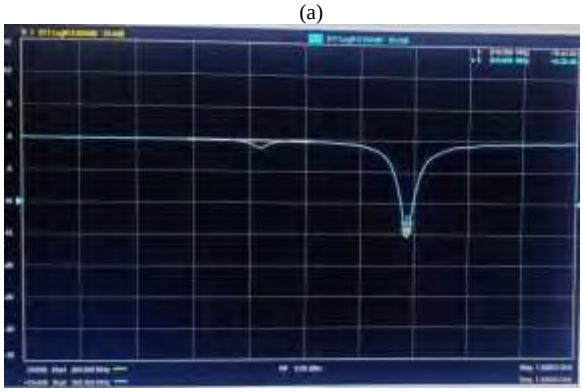

(b)

Fig. 10. Measured and simulated S11 of the proposed antenna a) diode ON b) diode OFF

The measured impedance bandwidth of the proposed antenna is 19 MHz at 866 MHz and 22 MHz at 916 MHz, which is sufficient to cover the IN865 and AS923-3 LoRa frequency bands [7]. To further evaluate the antenna's performance, the radiation characteristics, Co and Cross-polarization are shown in figure 11, where subplots (a)-(d) correspond to the diode ON state, subplots (e)-(h) represent the diode OFF state and (i)-(l) represent Co and Cross-polarization. The 2D radiation polar plots in the XZ-plane (H-cut) and XY-plane (E-cut), along with their 3D counterparts, are provided for both operating states. At 866 MHz, the measured peak gains are 2.07 dBi in the E-plane and 2.03 dBi in the H-plane, while at 916 MHz, the corresponding gains are 2.07 dBi and 1.98 dBi, respectively. In both resonance states, the major lobe is consistently directed at 277^{o}, demonstrating the stability of the antenna's radiation performance across both frequency bands. The results show that the co-polarized component dominates, while the cross-polarization levels remain significantly lower, confirming acceptable radiation performance of the proposed antenna. The simulated model exhibits good radiation efficiency of 86.2% (916 MHz) and 72.3% (866 MHz) as shown in figure 12, indicating minimal losses in the antenna structure.

The PIN diode introduces parasitic resistance, inductance, and capacitance, which affect both impedance and radiation characteristics. The series resistance leads to additional losses, slightly reducing radiation efficiency and gain, while the parasitic inductance and capacitance alter the current distribution on the radiating element, causing minor variations in the radiation pattern. Due to the electrically small size of the diode, these effects remain limited, as reflected in the stable gain and radiation patterns observed.

Table 6 Compares the Innovative aspects of the Proposed design with the several other related works in terms of design and dimensions. From the table, it is evident that while several antennas such as [10], [11], [12], and [15] are non-reconfigurable, recent designs like [17], [19], and [20] employ reconfiguration techniques to achieve multiband operation. However, these works do not specifically target the LoRa frequency bands considered in this study (IN865 and AS923-3). In addition, their overall antenna dimensions are significantly larger than the proposed design. Although [20] offers the desired radiation characteristics, it does so at the cost of increased size and circuit complexity. These approaches also typically require multiple PIN diodes or tunable capacitors, which increase biasing requirements, circuit complexity, and cost.

Though the proposed design achieves a gain of 2.07 dBi and a S11 of -15 to -17 dB, which are moderate compared to designs [10], [11], and [14], these values represent a practical trade-off to maintain a compact size ($42 \times 40 \times 1.6$ mm^3) and a simple reconfiguration network. The antenna also exhibits stable radiation patterns, and the measured bandwidths sufficiently cover the target LoRa bands, offering a balanced and reliable solution for IoT deployments.

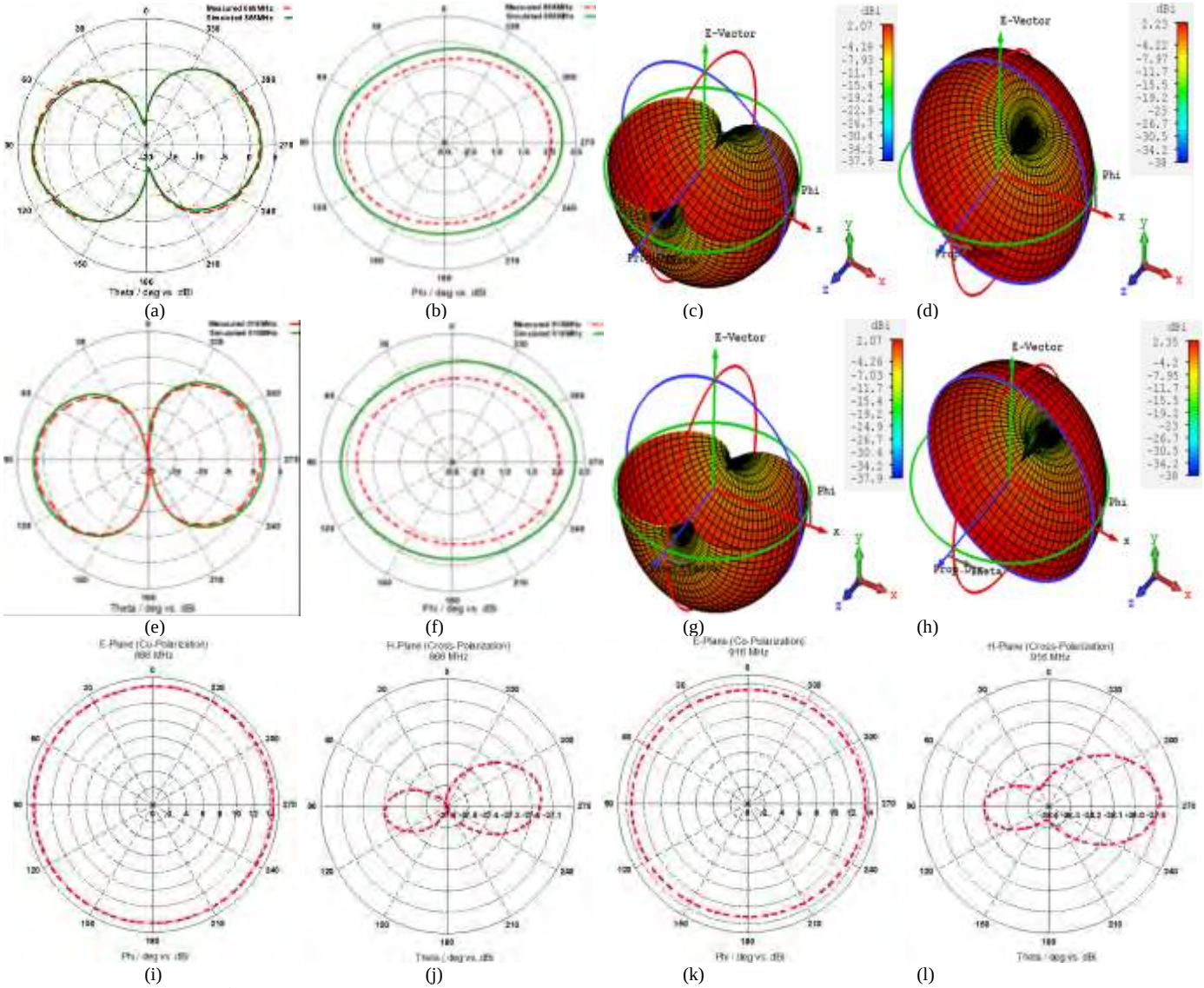

Fig. 11. Radiation patterns of the proposed antenna a) 2D H-cut (XZ-Plane) with diode ON b) 2D E-cut (XY-Plane) with diode ON c) 3D H-cut with diode ON d) 3D E-cut with diode ON e) 2D H-cut (XZ-Plane) with diode OFF b) 2D E-cut (XY-Plane) with diode OFF c) 3D H-cut with diode OFF d) 3D E-cut with diode OFF i) Co-Polarization at 866MHz j) Cross-Polarization at 866MHz k) Co-Polarization at 916MHz l) Cross-Polarization at 916MHz

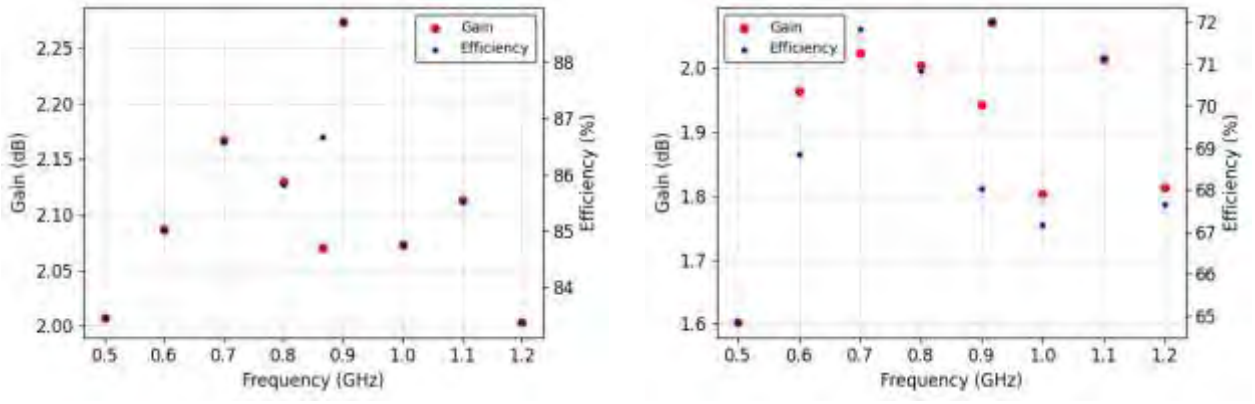

Fig. 12 Efficiency, Gain vs. Frequency plot a) diode ON b) diode OFF

TABLE VI
COMPARISON OF PROPOSED DESIGN WITH RELATED WORKS

Related works	Size (mm)	Substrate	Frequency (MHz)	Gain (dBi)	S11 (dB) (approx.)	Bandwidth	LoRa Only Multiband	Reconfiguration method	Pattern Stability (major lobe)
[10]	13.1x22.9x1.6	FR-4	923	-11.86	-10	4.5 MHz	NA	NA	NA
[11]	125×20×1.6	FR-4	433	-6.00	-12	38 MHz	NA	NA	NA
[12]	57.9x45.1x1.6	FR-4	871	0.58	-20	28 MHz	NA	NA	NA
[13]	82.6x44x1.6	FR-4	867 (LoRa),	1.78	-21	15 MHz	No	Non-	Yes (0º)
			1500 (UMTS)	3.80	-24	80 MHz		Reconfigurable	
[14]	65×62×1.6	FR-4	868 (LoRa),	3.35	-16	10 MHz	No	Non-	No (180º,0º)
			1575 (GPS)	5.08	-32	47 MHz		Reconfigurable	
[15]	98.8x77.2x1.6	FR-4	922.5	1.04	-21	22 MHz	NA	NA	NA
[16]	102x81x1.6	FR-4	866 (LoRa),	-2.00	-34	10 MHz	No	Non-	Partial (0º, 30º)
			937 (GSM)	-3.00	-32	15 MHz		Reconfigurable	
[17]	78×88×1.6	FR-4	868 (LoRa),	-2.50	-22	---	No	1-PIN Diode	------
			401 & 466	-8.50	-14				
			(Sat com.)	-5.20	-26				
[18]	22×34×0.5	FR-4	868 (LoRa)	2.56	-12	930 MHz	Yes	Non-	------
			915 (LoRa)	2.10	-10			Reconfigurable	
[19]	70x70x0.78	Rogers	868 (LoRa)	0.20	-10	6 MHz	No	Digital Tuneable	No (90º, 0º, 0º)
		RO5880	1580 (GPS)	1.80	-25	10 MHz		Capacitor	
			2400 BLE	5.70	-11	10 MHz			
[20]	80x50x1.6	FR-4	868 (LoRa)	2.01	-19	---	Yes	3-PIN Diodes	Yes (180º)
			915 (LoRa)	2.10	-30				
			915 & 433	1.98	-25				
Proposed work	42x40x1.6	FR-4	866 (LoRa)	2.07	-17	19 MHz	Yes	1-PIN Diode	Yes (277º)
			916 (LoRa)	2.07	-15	22 MHz			

V. CONCLUSION

In this paper, we present a compact, cost-effective reconfigurable MMA designed for operation in the LoRa IN865 and AS923-3 bands. The design incorporates a meandered monopole structure along with an RF PIN diode, resulting in a compact and economical solution. The proposed antenna is tuned to operate at the target central frequencies of the LoRa bands. The antenna is fabricated on an FR-4 substrate of size 42 mm × 40 mm with a thickness of 1.6 mm. An RF PIN diode (BAR50-02V), which operates on 3.0 V DC, has been employed in the design to switch between the two LoRa bands. Simulation results conducted using CST-MWS demonstrate that the antenna achieves a gain of 2.07 dBi with stable radiation patterns and switches between the frequencies 866.8 MHz and 916.9 MHz with S11 values of -15.32 dB and -14.38 dB, respectively. These results are corroborated by measurements taken from the prototyped version of the antenna. Moreover, the lumped equivalent model developed using Keysight ADS provides a simplified and accurate representation of the antenna behavior, further confirming its efficiency. Overall, the proposed reconfigurable meandered monopole antenna offers a compact, cost-effective solution with significant potential for enhancing IoT communication networks in the targeted regions.

REFERENCES

[1] A. Hoeller, R. D. Souza, O. L. A. Lopez, H. Alves, M. De Noronha Neto, and G. Brante, "Analysis and performance optimization of LoRa networks with time and antenna diversity," IEEE Access, vol. 6, pp. 32820–32829, Jan. 2018, doi: 10.1109/ACCESS.2018.2839064.

[2] F. Duarte, "Number of IoT devices (2024)," Exploding Topics, Feb. 19, 2024. [Online]. Available: https://explodingtopics.com/blog/number-of-iot-devices, Accessed: May 2026.

[3] A. Celik, I. Romdhane, G. Kaddoum, and A. M. Eltawil, "A top-down survey on optical wireless communications for the Internet of Things," IEEE Commun. Surveys Tuts., vol. 25, no. 1, pp. 1–45, Nov. 2022, doi: 10.1109/COMST.2022.3220504.

[4] A. Khalifeh et al., "A new approach towards LoRa wireless technology parameters' selection," in Proc. IEEE Jordan Int. Joint Conf. Electr. Eng. Inf. Technol. (JEEIT), 2019, pp. 283–287, doi: 10.1109/JEEIT53412.2021.9634147.

[5] R. B. Khanderay and O. Kemkar, "Analysis of LoRa framework in IoT technology," in Proc. Int. Conf., 2021, pp. 1–4, doi: 10.1109/AIMV53313.2021.9670961.

[6] H. Kurt and A. Kaya, “Triband microstrip rectangular patch antenna for Bluetooth/WiFi applications,” ICONTECH Int. J., vol. 6, no. 1, pp. 58–62, Mar. 2022, doi: 10.46291/icontechvol6iss1pp58-62.
[7] “RP002-1.0.2 LoRaWAN regional parameters,” 2020. [Online]. Available: https://lora-alliance.org/wp-content/uploads/2020/11/RP_2-1.0.2.pdf, Accessed: May 2026.
[8] X. Guo et al., “Efficient ambient LoRa backscatter with on-off keying modulation,” IEEE/ACM Trans. Netw., vol. 30, no. 2, pp. 641–654, Nov. 2021, doi: 10.1109/TNET.2021.3121787.
[9] N. Jovalekic, V. Drndarevic, E. Pietrosemoli, I. Darby, and M. Zennaro, “Experimental study of LoRa transmission over seawater,” Sensors, vol. 18, no. 9, p. 2853, Aug. 2018, doi: 10.3390/s18092853.
[10] W. Wanpare, A. Paisal, and S. Chalermwisutkul, “A compact 923 MHz monopole antenna for LoRaWAN IoT applications,” in Proc. IEEE Conf., 2020, pp. 53–56, doi: 10.1109/ICPEI49860.2020.9431578.
[11] N. Q. Zhang and N. Y. Gao, “Embedded antenna design on LoRa radio for IoT applications,” in Proc. Eur. Conf. Antennas Propag. (EuCAP), 2018, pp. 1–3, doi: 10.1049/cp.2018.0920.
[12] A. Pandey and M. V. D. Nair, “Inset fed miniaturized antenna with defected ground plane for LoRa applications,” Procedia Comput. Sci., vol. 171, pp. 2115–2120, 2020, doi: 10.1016/j.procs.2020.04.228.
[13] A. D. Boursianis et al., “Multiband patch antenna design using nature-inspired optimization method,” IEEE Open J. Antennas Propag., vol. 2, pp. 151–162, Dec. 2020, doi: 10.1109/OJAP.2020.3048495.
[14] M. S. Yahya et al., “Dual-band GPS/LoRa antenna for Internet of Things applications,” Bull. Electr. Eng. Informat., vol. 13, no. 2, pp. 986–995, Feb. 2024, doi: 10.11591/eei.v13i2.6428.
[15] P. Wounchoum, A. Kongsavat, and C. Karupongsiri, “Designing and implementing a microstrip antenna on LoRa frequency for smart meter communication,” Electron. ETF, vol. 26, no. 1, pp. 9–16, Jun. 2022, doi: 10.53314/els2226009w.
[16] Low-cost dual-band e-shaped patch antenna for energy harvesting applications using Grey Wolf optimizer,” IEEE Xplore, Mar. 2019. [Online]. Available: https://ieeexplore.ieee.org/document/8739560, Accessed: May 2026.
[17] A. Bouyedda, B. Barelaud, and L. Gineste, “Design and realization of a UHF frequency reconfigurable antenna for hybrid connectivity LPWAN and LEO satellite networks,” Sensors, vol. 21, no. 16, p. 5466, Aug. 2021, doi: 10.3390/s21165466.
[18] R. Roges, P. K. Malik, and S. Sharma, “A compact wideband antenna with DGS for IoT applications using LoRa technology,” in Proc. Int. Conf. Emerg. Trends Eng. Technol. Signal Inf. Process. (ICETET-SIP), 2022, pp. 1–4, doi: 10.1109/ICETET-SIP2254415.2022.9791725.
[19] F. A. Asadallah et al., “A digitally tuned reconfigurable patch antenna for IoT devices,” in Proc. IEEE Conf., 2017, doi: 10.1109/APUSNCURSINRSM.2017.8072501.
[20] M. S. Yahya et al., “A compact reconfigurable multi-frequency patch antenna for LoRa IoT applications,” Prog. Electromagn. Res. M, vol. 116, pp. 77–89, Jan. 2023, doi: 10.2528/PIERM23021804.
[21] H. H. M. Ghouz, M. F. A. Sree, and M. A. Ibrahim, “Novel wideband microstrip monopole antenna designs for WiFi/LTE/WiMax devices,” IEEE Access, vol. 8, pp. 9532–9539, 2020, doi: 10.1109/ACCESS.2019.2963644.
[22] O. P. N. Calla et al., “Empirical relation for designing the meander line antenna,” in Proc. Int. Conf. Recent Adv. Microw. Theory Appl., 2008, pp. 695–697, doi: 10.1109/AMTA.2008.4762995.
[23] P. Kaur, “Design of compact and broadband rectangular patch antenna using cylindrical rods artificial dielectric,” Int. J. Inf. Technol., vol. 14, no. 3, pp. 1405–1414, Mar. 2021, doi: 10.1007/s41870-021-00624-y.
[24] S. Shanmuganathan et al., “Design and analysis of sub-1 GHz antenna for non-standalone vehicular communication,” Sci. Rep., vol. 15, no. 1, Jul. 2025, doi: 10.1038/s41598-025-07188-y.

Pothala Chaya Devi received her Bachelor of Technology Degree in Electronics and Communication Engineering from JNTU Kakinada in 2012 and M. Tech Degree in Radar and Microwave Engineering from Andhra University in 2014. She had published 23 articles in various International and National Journals and Conferences. She is presently working as Assistant Professor in Department of ECE in Anil Neerukonda Institute of Technology and Sciences. Her research interest includes design of microstrip antenna, implantable antenna for RF and Wireless communication systems, and Machine Learning.

Ramarakula Madhu received the BE (Bachelor of Engineering) degree in electronics and communication engineering from Osmania University, Hyderabad, India, in 2003 and MTech degree in communication systems from Jawaharlal Nehru Technological University Hyderabad, India, in 2009. He received his PhD degree in electronics and communication engineering from Andhra University, Visakhapatnam, India, in 2014. He is presently working as an assistant professor in the Department of Electronics and Communication Engineering, University College of Engineering Kakinada (A), JNTUK, Kakinada, India. He has 10 years of teaching experience. He has published more than 40 research papers in various reputed national and international journals and conferences. His research interests include mobile and cellular communications, antennas, satellite communications, and GNSS. He is a Member of IEEE.